

## Luminescence in Mn-doped CdS nanocrystals

ANGSHUMAN NAG<sup>1</sup>, SAMEER SAPRA<sup>1</sup>, SUBHRA SEN GUPTA<sup>1</sup>, ANKITA PRAKASH<sup>1</sup>, AJIT GHANGREKAR<sup>2</sup>, N PERIASAMY<sup>2</sup> and D D SARMA<sup>1,3,\*</sup>

<sup>1</sup>Solid State and Structural Chemistry Unit, Indian Institute of Science, Bangalore 560 012, India

<sup>2</sup>Department of Chemical Sciences, Tata Institute of Fundamental Research, Mumbai 400 005, India

<sup>3</sup>Centre for Advanced Materials, Indian Association for the Cultivation of Science, Kolkata 700 032, India

**Abstract.** We have synthesized Mn-doped CdS nanocrystals (NCs) with size ranging from 1.8–3 nm. Photoluminescence (PL) spectra of the doped NCs differ from that of the undoped NCs with an additional peak due to Mn *d-d* transitions. Electron paramagnetic resonance spectra along with X-ray absorption spectroscopy and PL spectra confirm the incorporation of Mn in the CdS lattice. The fact that emissions from surface states and the Mn *d* levels occur at two different energies, allowed us to study the PL lifetime decay behaviour of both kinds of emissions.

**Keywords.** Luminescence; doping; semiconductor nanocrystals.

### 1. Introduction

Doped semiconductor nanocrystals are being studied intensively to achieve two different material properties, viz. luminescence and magnetism. The impurity atoms doped sparsely into nanocrystals provide sharp atomic levels for capturing the excited electrons and holes, formed upon excitation of particles across the band gap, from the host semiconductor lattice and displaying narrow emission spectra due to recombination of electrons and holes between these sharp levels. If the impurity atoms have unfilled *d* electrons, then one also observes the magnetic properties. Either or both of these properties have been studied in a few Mn-doped semiconductors such as Cd<sub>1-x</sub>Mn<sub>x</sub>S (Levy *et al* 1996; Counio *et al* 1998; Feltin *et al* 1999; Nag *et al* 2007), Zn<sub>1-x</sub>Mn<sub>x</sub>S (Wang *et al* 1991; Bhargava *et al* 1994; Soo *et al* 1994; Sapra *et al* 2003), Cd<sub>1-x</sub>Mn<sub>x</sub>Se (Erwin *et al* 2005), Zn<sub>1-x</sub>Mn<sub>x</sub>Se (Pradhan and Peng 2007), Zn<sub>1-x</sub>Mn<sub>x</sub>O (Viswanatha *et al* 2004), Ga<sub>1-x</sub>Mn<sub>x</sub>As and In<sub>1-x</sub>Mn<sub>x</sub>As (Ohno 1998, 1999).

Manganese-doped CdS nanocrystals have been mainly studied due to their luminescence properties. This is due to the fact that the doped Mn<sup>2+</sup> ions provide good traps for the excited electrons though the Mn spins do not align to give magnetic behaviour in the case of bulk Cd<sub>1-x</sub>Mn<sub>x</sub>S; it gives rise to paramagnetism (Furdyna 1988). However, in the nanocrystalline phase, Hoffman and coworkers (2000) have reported the presence of a giant internal magnetic field, with a commensurate Zeeman splitting of the electron and hole levels as high as 100 meV. Mn<sup>2+</sup> ion emission has been reported at ~590 nm (Wang *et al* 1991;

Bhargava *et al* 1994; Soo *et al* 1994; Levy *et al* 1996; Counio *et al* 1998; Feltin *et al* 1999; Sapra *et al* 2003; Erwin *et al* 2005; Nag *et al* 2007; Pradhan and Peng 2007). The excited electrons are transferred from the conduction band to the Mn *d* levels through which the radiative de-excitation occurs via <sup>4</sup>T<sub>1</sub>–<sup>6</sup>A<sub>1</sub> transitions. This is observed as the orange emission. Earlier reports show a broad band apart from the orange band in the doped and undoped CdS nanocrystals at a wavelength higher than 600 nm. This has been attributed to defect or surface related emission. In the present report, we observe this emission at wavelength lower than the Mn emission. We attribute this emission to the defect states and the observation of this emission at a higher energy to the difference in the method of synthesis and is described below in the discussion on fluorescence studies.

### 2. Experimental and methods

The chemicals were used as received without further purification. Cd(OAc)<sub>2</sub>·2H<sub>2</sub>O, Mn(OAc)<sub>2</sub>·4H<sub>2</sub>O and solvent dimethyl sulphoxide (DMSO) were purchased from Ranbaxy. Na<sub>2</sub>S·9H<sub>2</sub>O was obtained from Aldrich and the capping agent, 1-thioglycerol, from Fluka. Double distilled water was employed for all the reactions. Synthesis procedure was borrowed from Nag *et al* (2007) but with a desired change in the reaction temperatures. A typical synthesis involved dissolution of Cd<sup>2+</sup> (4-*y* mmol) and Mn<sup>2+</sup> (*y* mmol) salts in 40 ml DMSO and 0.5 ml thioglycerol was added to this solution. The quantity, *y*, was equated to the Mn percentage, *x* as in Cd<sub>1-x</sub>Mn<sub>x</sub>S, using the formula  $x = (y/4)$ . A separate solution of S<sup>2-</sup> in 10 ml water was freshly prepared and added drop by drop to the DMSO solution over a period of ~5 min. Then the reaction

\*Author for correspondence (sarma@sscu.iisc.ernet.in)

mixture was heated to the desired temperature for 12 h. Acetone was added to the reaction mixture to precipitate the nanocrystals which were then washed with methanol several times to remove the adhering unreacted reagents. Dilute solutions in DMSO–water mixture were prepared for UV-Vis and fluorescence studies.

UV-Vis absorption experiments were performed on a Perkin Elmer's Lambda 35 UV/visible spectrometer at a bandwidth of 2 nm. Fluorescence emission was recorded on a Perkin Elmer LS 55 with the excitation and emission slits at 5 nm each. Excitation was carried out at 370 nm. Powder X-ray diffraction (XRD) patterns were recorded on a Siemens D5005 X-ray diffractometer at 1.2° per min. Electron paramagnetic resonance (EPR) spectra were measured on powder samples in a quartz tube. X-ray absorption spectra (XAS) were recorded at the BEAR beamline at Sincrotrone centre, Elettra, Trieste, Italy.

The theoretical  $2p \rightarrow 3d$  XAS of Mn in Mn-doped CdS was calculated using the Lanczos iterative algorithm for a many-body Hamiltonian, based on a fully coherent spectral function for the  $(\text{MnS}_4)^{6-}$  tetrahedral cluster corresponding to the zinc-blende or the wurtzite structure. The details of the Hamiltonian involved and the method of calculation are discussed elsewhere (Mahadevan and Sarma 2000). The calculations were performed with complete Mn  $3d-3d$  and  $2p-3d$  multiplet interactions, corresponding to average values ( $U_{dd}$  and  $U_{pd}$ ) of 5.8 eV and 7 eV, respectively (Bocquet *et al* 1992). The hopping parameters used for MnS were S–S ( $pp\sigma$ ) = 0.32 eV, S–S ( $pp\pi$ ) = -0.04 eV, S–Mn ( $pd\sigma$ ) = -1.64 eV, and S–Mn ( $pd\pi$ ) = 0.42 eV. The charge transfer energy ( $\Delta$  = 5 eV) and the crystal field ( $T_d$ ) strength (10 Dq = 0.4 eV), were adjusted to obtain the best description of the experimental data. The spectrum thus obtained was broadened by a Gaussian function of width, 0.5 eV, to simulate instrumental broadening and a Lorentzian function of width, 0.55 eV, to account for the finite lifetime of the core hole.

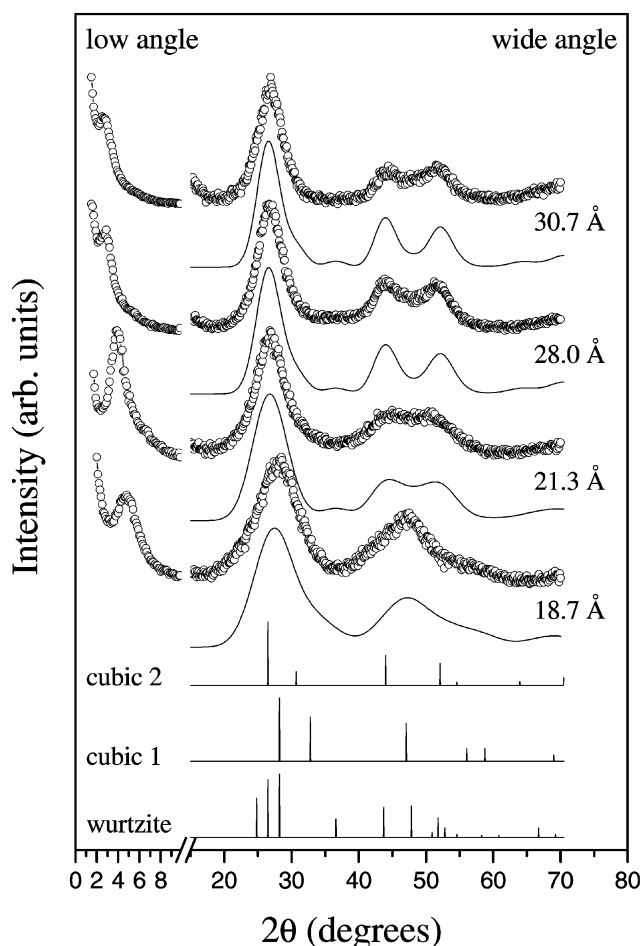
### 3. Results and discussion

Figure 1 shows the low and wide-angle X-ray diffraction (XRD) patterns of nanocrystals of CdS synthesized at 60°C, 100°C, 130°C and 160°C. Also shown are the XRD patterns of bulk CdS in the wurtzite and zinc-blende structure. Upon decreasing the reaction temperature, one observes that the XRD peaks get broader. This indicates that the size of the nanocrystals is small when grown at lower temperatures, whereas higher temperatures yield larger sized particles. The diameter,  $D$ , of the nanocrystals can be determined using the Scherrer formula (Guinier 1963)

$$D = \frac{4}{3} \frac{0.9\lambda}{B \cos\theta}, \quad (1)$$

where  $B$  is the full-width at half maximum (FWHM) of the XRD peak at  $2\theta$ , recorded with an incident wavelength,

$\lambda$ . The bulk XRD pattern is broadened to an amount determined by the variable parameter,  $B$ , to get the best description of the nanocrystal XRD pattern. This tells us about the size of the nanocrystals. These sizes are tabulated in table 1. The bulk patterns that are broadened and compared with the experimental results are shown in the bottom of the figure. No single broadened bulk pattern can match any of the experimental patterns. Hence, we



**Figure 1.** Low angle and wide angle X-ray diffraction patterns for undoped CdS nanocrystals synthesized at 60°C, 100°C, 130°C and 160°C. The bulk patterns for cubic (cubic 1 and cubic 2) and wurtzite, that are used for broadening, are shown at the bottom of the figure. Below each wide angle XRD, the corresponding broadened pattern is also shown.

**Table 1.** Sizes obtained from different characterization techniques. All values are in Ångströms.

Temperature (°C)	Wide angle XRD	Low angle XRD	UV-Vis
60	18.7	18.4	19.5
100	21.3	22.6	22.5
130	28.0	30.4	27.7
160	30.7	35.3	30.0

used a superposition of the broadened bulk patterns in varying proportions to obtain an agreement with the experimental data. It is found that the samples made at higher temperatures, 100°C, 130°C and 160°C, are a mixture of the cubic zinc blende (cubic 2) and the hexagonal wurtzite structure. The samples prepared at 60°C crystallize in the zinc-blende structure, though they are a mixture of two cubic structures viz. cubic 1 (space group:  $Fm\bar{3}m$ ) and cubic 2 (space group:  $F\bar{4}3m$ ) as shown in the figure. It has been shown earlier that phase transformations occur at very small nanocrystal sizes (Vossmeier *et al* 1994).

The nanocrystals tend to organize themselves into ordered structures. This gives rise to diffraction peaks in the very low angle regime, corresponding to the average distance between the nanocrystals. The left part of figure 1 shows the low angle diffraction peaks from the four different samples. The distance between two nanocrystal centres corresponding to the low angle peak is given by the Bragg's Law. From the low angle peaks for the CdS, the sizes calculated for the samples synthesized at various temperatures are listed in table 1. The values are in good agreement with those obtained from wide angle XRD.

The XRD patterns do not change upon doping Mn<sup>2+</sup> ions into the CdS nanocrystals. This is shown by the wide angle X-ray diffraction patterns for Cd<sub>1-x</sub>Mn<sub>x</sub>S nanocrystals in figure 2.

Figure 3 shows the UV-Vis spectra of the four CdS samples synthesized at different temperatures. We notice a systematic shift in the absorption edge, away from bulk CdS, as the synthesis temperature is lowered. As already seen from the XRD analysis, the size of the nanocrystals decreases as the reaction temperature is decreased. Thus, due to the quantum confinement effect, the bandgap of the nanocrystals, which is determined from the UV-Vis spectra, increases with a decrease in the particle size. The nanocrystal size can be determined from the bandgap shift seen in the absorption spectra by comparing it with theoretical models. The most accurate model for determining the electronic structure of II-VI nanocrystals uses the tight-binding approximation with the  $sp^3d^5$  orbital basis and next nearest neighbour interactions between the anions and the cations (Sapra *et al* 2002; Sapra and Sarma 2004). The sizes obtained from the bandgap variation versus size curve for CdS in Sapra and Sarma (2004) are listed in table 1. The values are in good agreement

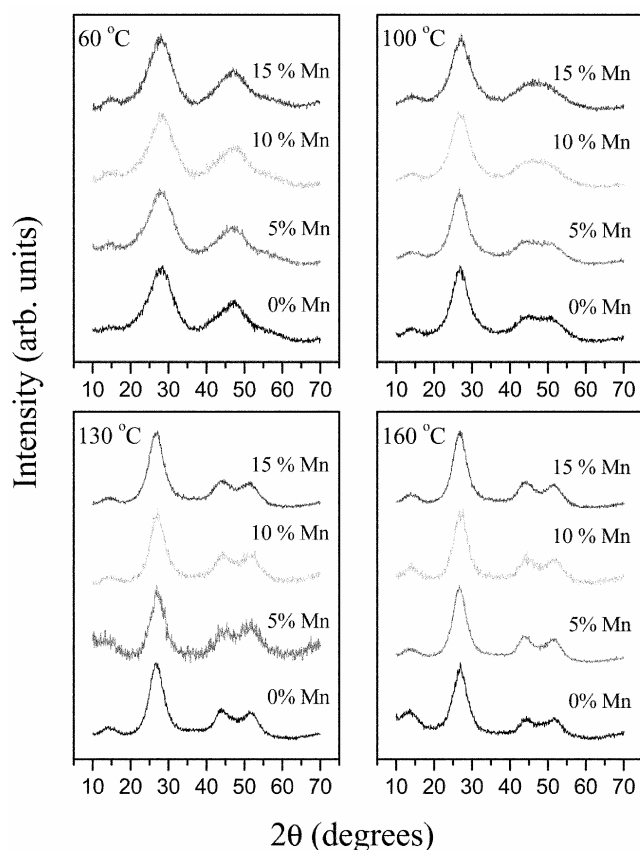


**Figure 2.** Wide angle X-ray diffraction patterns for varying amounts of Mn in Mn-doped CdS nanocrystals synthesized at different temperatures. The broad peak around 14 degree is due to the amorphous glass substrate used as a sample holder.

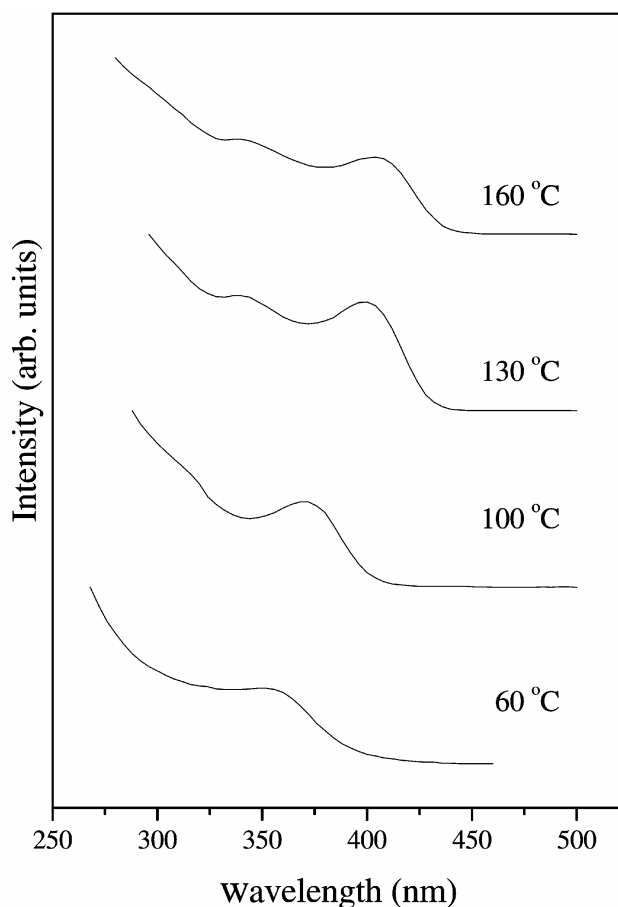


**Figure 3.** UV-Vis absorption spectra for undoped CdS nanocrystals synthesized at various temperatures.

with those obtained from the wide and low angle XRD patterns, similar to the ones reported earlier (Nag *et al* 2007). However, we notice that the size estimate from the low angle XRD patterns is slightly larger compared to the size estimate from the UV-Vis absorption spectra except for the smallest sized clusters. We attribute it to the fact that the lower temperature used (60°C) for synthesizing the small sized sample gives a rather large size distribution and hence the UV-Vis spectrum has a tail towards the higher wavelength owing to the presence of larger nanocrystals obtained in this synthesis technique, thus giving a slightly larger size estimate. Analogous to Nag *et al* (2007), the UV-Vis absorption spectra for identically sized Mn-doped CdS nanocrystals with various Mn percentages (not shown here) indicate that Mn-doping does not change the size of the nanocrystals thus, enabling us to study the properties of fixed size nanocrystals with varying doping concentrations.

Mn-doping into semiconductor nanocrystals has been a topic of debate for the past few years (Wang *et al* 1991; Bhargava *et al* 1994; Soo *et al* 1994; Levy *et al* 1996; Counio *et al* 1998; Feltin *et al* 1999; Sapra *et al* 2003; Erwin *et al* 2005; Nag *et al* 2007; Pradhan and Peng 2007).

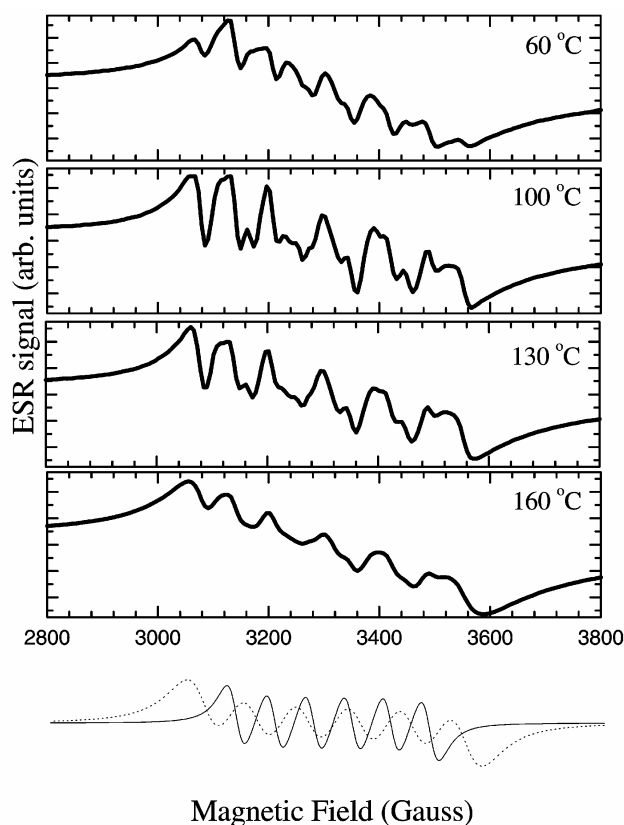


**Figure 4.** Electron paramagnetic resonance spectra for Mn doped CdS nanocrystals synthesized at different temperatures. The nominal amount of Mn is 10%. At the bottom of the figure the two components with splitting of 69 and 90 Gauss are shown.

Techniques such as X-ray diffraction, electron paramagnetic resonance, EXAFS and fluorescence emission have been employed to establish the presence of Mn centres in the nanocrystal lattice. Although lattice dilation upon incorporation of impurity atoms is conclusive to establish the presence of Mn inside the nanocrystals, the other methods are not as conclusive, though they are indicative. In case of very small sized nanocrystals, where the XRD peaks are broad, and in addition, the amount of dopant is very small, it is impossible to determine the shifts in the XRD pattern. However, a careful preparation of the sample and detection of the presence of Mn using various techniques can establish the Mn centres being present in the host CdS nanocrystal.

The presence of Mn ions in the nanocrystals is evidenced from the EPR spectra shown in figure 4. The figure shows the EPR spectra of different sized CdS nanocrystals doped with varying amounts of Mn. The spectra suggest a multiple finger pattern characteristic of the  $\text{Mn}^{2+}$  species. Thus, one can confidently state that  $\text{Mn}^{2+}$  ions are present in the nanocrystals. Moreover, these  $\text{Mn}^{2+}$  ions are spatially isolated because we observe the sextet patterns; clustered  $\text{Mn}^{2+}$  ions give rise to broad and featureless EPR spectra due to Mn–Mn interactions (Sapra *et al* 2003). A closer inspection of the EPR spectra shows that the spectra itself is composed of at least two different types of signals. This can be attributed to the fact that  $\text{Mn}^{2+}$  ions are present in different environments (Nag *et al* 2007). Inside the nanocrystals the  $\text{Mn}^{2+}$  ions can substitute for the  $\text{Cd}^{2+}$  ions which are tetrahedrally coordinated. If  $\text{Mn}^{2+}$  ions are present on the surface of the nanocrystals, then they would prefer the octahedral coordination. The tetrahedral coordination gives rise to an EPR sextet with a peak-to-peak separation of 69 Gauss and the octahedral environment leads to an approximately 90 Gauss separation. Both these components are present in the EPR spectra recorded from the  $\text{Cd}_{1-x}\text{Mn}_x\text{S}$  samples, similar to those reported earlier (Nag *et al* 2007). The individual components are also shown in the bottom part of the figure. We notice that the samples synthesized at 60°C have the maximum amount of the 69 Gauss component which decreases as we go towards samples synthesized at higher temperatures. We believe that higher synthesis temperatures drive the  $\text{Mn}^{2+}$  ions towards the surface of the nanocrystals.

We have employed yet another method to establish the presence of  $\text{Mn}^{2+}$  ions in CdS nanocrystals. X-ray absorption spectroscopy (XAS) is a useful technique to study the local environment (coordination) and oxidation state of various ions. In particular, the transition metal ions have been well characterized (van der Laan and Kirkman 1992). Figure 5 shows the XAS for the Mn  $L_3$  edge for the highest doped samples as specified in the figure. The spectral shape resembles that of  $\text{Mn}^{2+}$  ions in the interior of ZnO nanocrystals (Mikulec *et al* 2000). In order to determine the valency, symmetry, and the crystal field strength of

the  $\text{Mn}^{2+}$  ions in the present case, we carried out theoretical calculations for various crystal field strengths. The spectrum that gives the best description of the experimental spectrum corresponds to a  $\text{Mn}^{2+}$  species in a tetrahedral symmetry ( $10 Dq = 0.4 \text{ eV}$ ) and is shown in the figure with a solid line, evidently providing a good agreement with the experimental data. However, we must point out that even the octahedral symmetry with the same crystal field strength provides an equally good description to the experimental spectrum (van der Laan and Kirkman 1992). Thus,  $\text{Mn}^{2+}$  ions can be inside or at the surface of the nanocrystals and could not distinguish between the two kinds of  $\text{Mn}^{2+}$  species. It is interesting to note that the characteristic Mn  $2p$  spectrum for a tetrahedrally coordinated  $\text{Mn}^{2+}$  ion is observed only in the case of the highest doped sample. Thus, even 20% nominal  $\text{Mn}^{2+}$  doping gives a very low concentration of  $\text{Mn}^{2+}$  ions in the nanocrystals.

Figure 6 shows the fluorescence emission spectra of undoped and Mn-doped CdS nanocrystals with different amounts of Mn concentration, synthesized at different temperatures. The excitation wavelengths used are at the absorption band edges of the respective samples. Un-

doped sample synthesized at  $60^\circ\text{C}$  shows a broad peak centred at about  $500 \text{ nm}$ , similar to the one reported earlier (Nag *et al* 2007). This emission is the result of radiative recombination of the electrons and holes via the surface/defect states present in the nanocrystals. The electrons and holes, after excitation across the band edge, trickle down non-radiatively to the surface states lying in the bandgap region. Radiative de-excitation across the surface states in CdS nanocrystals gives rise to bright yellow–green fluorescence observed at around  $500 \text{ nm}$ . The fluorescence emission maxima shift towards higher wavelength upon increasing the nanocrystal size due to the fact that the bandgap decreases upon increasing the size consequently leading to a decrease in the energy difference between the surface states through which the electrons and holes de-excite radiatively.

Mn  $d$  levels provide a channel for de-excitation of electrons and holes other than the surface states. As the Mn  $d$  levels lie in the bandgap region they can readily capture the excited electrons from the the band edge as well as surface states (Sapra *et al* 2005). The characteristic  $\text{Mn}^{2+}$  emission occurs at  $\sim 590 \text{ nm}$  owing to the  ${}^4T_1 - {}^6A_1$  transition. Doping CdS nanocrystals with  $\text{Mn}^{2+}$  ions, synthesized at  $60^\circ\text{C}$  gives rise to a second peak in the emission spectrum as seen in the upper panel of figure 6, similar to the one reported earlier (Nag *et al* 2007). Thus, we know

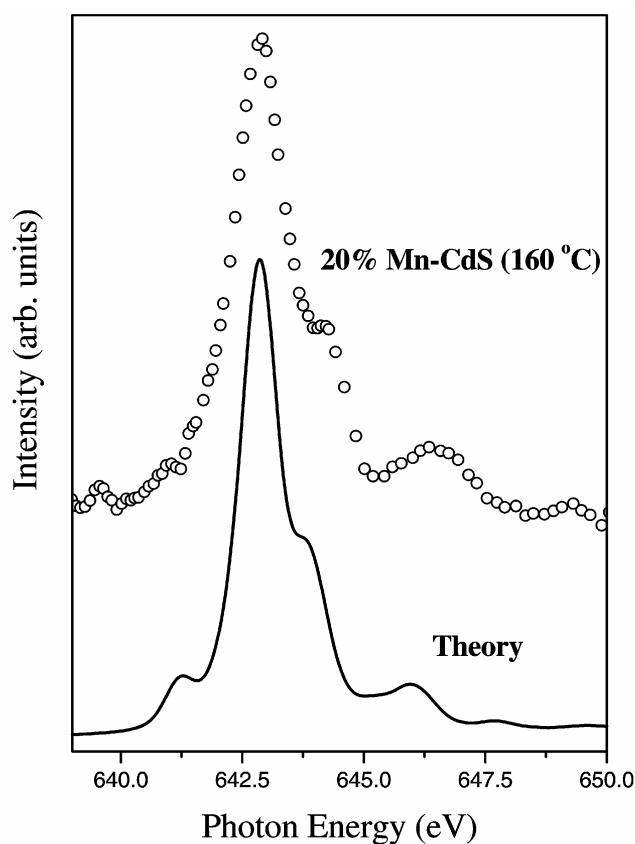


**Figure 5.** X-ray absorption for the Mn  $L_3$  edge for the highest concentration of Mn doping in the sample synthesized at  $160^\circ\text{C}$ . Also shown is the calculated XAS for  $(\text{MnS}_4)^{6-}$  tetrahedral cluster as described in the text.

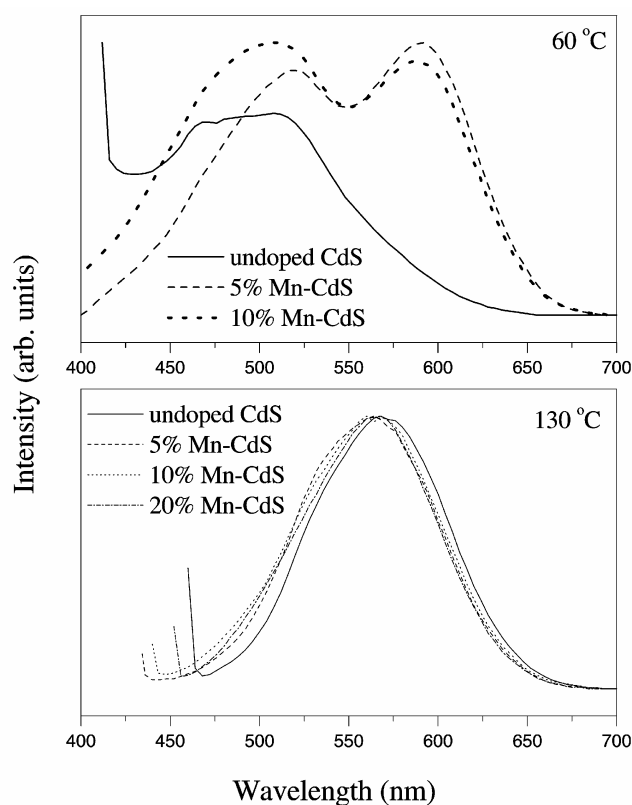


**Figure 6.** Fluorescence spectra for undoped and Mn-doped CdS nanocrystals synthesized at  $60^\circ\text{C}$  and  $130^\circ\text{C}$ .

that  $\text{Mn}^{2+}$  ions are doped into the CdS lattice as the Mn  $d$  levels couple to the CdS electronic states and the excited electrons de-excite via the Mn  $d$  states giving rise to a bright orange fluorescence. As the size of the  $\text{Cd}_{1-x}\text{Mn}_x\text{S}$  nanocrystals increases upon increasing the temperature, the fluorescence emission through the surface states shifts to higher wavelengths. This leads to an overlap of the Mn  $d$  levels with the surface states and thus we do not observe any separate, well-resolved Mn emission peaks in samples synthesized at  $130^\circ\text{C}$ . The results are different from those reported earlier. Levy *et al* (1996) observe the surface state emission at wavelengths higher than 590 nm. This cannot be attributed to quantum confinement, since their nanocrystals are of the same size as reported here. We notice a difference in the synthesis methods. Levy *et al* (1996) used an excess of sulfide ions whereas we used an excess of cadmium ions. Thus, it is reasonable to argue that dangling cadmium bonds, as are present in our case are shallow surface states and thus exhibit emission at a higher energy whereas dangling sulfur bonds are rather deep states that give rise to red-shifted emission. Counio *et al* (1998) used stoichiometric amounts of cadmium and sulfur ions. They also observed an emission band at an energy lower than that of Mn emission. They attribute it to deep surface trap recombinations which are most likely from defect related states. Thus, in the present system, it is quite likely that the Mn steals some emission intensity from the surface states at higher energy as has been reported for the case of  $\text{Zn}_{1-x}\text{Mn}_x\text{S}$  nanocrystals recently (Sapra *et al* 2005).

To study the nature of the various states involved in fluorescence, lifetime decay studies are very useful. However, it is difficult to isolate the contribution from the various decay channels present in  $\text{Cd}_{1-x}\text{Mn}_x\text{S}$  nanocrystals, since both the surface states and the Mn  $d$  levels emit at the same energy for most of the samples reported in the literature so far. In the case of  $\text{Zn}_{1-x}\text{Mn}_x\text{S}$  nanocrystals (Sapra *et al* 2005), the emissions from surface states and the Mn  $d$  levels occur at very different energies. For  $\text{Cd}_{1-x}\text{Mn}_x\text{S}$  nanocrystals, we have been able to separate the two emissions by synthesizing smaller sized particles by carrying out the reaction at  $60^\circ\text{C}$ . Thus, the surface state emission, which is around 570 nm for the samples synthesized at higher temperatures, moves to 510 nm in the case of samples synthesized at  $60^\circ\text{C}$  as seen in figure 6. We have carried out fluorescence decay studies for the samples synthesized at  $60^\circ\text{C}$  with varying Mn content. We discuss the results of these measurements. Figure 7 shows the fluorescence decay curves of the undoped, 5 and 10% doped  $\text{Cd}_{1-x}\text{Mn}_x\text{S}$  nanocrystals measured at an emission wavelength of 510 nm. This corresponds to the peak of the surface state emission in the samples synthesized at  $60^\circ\text{C}$ . Here we notice the shortening of the 510 nm fluorescence emission lifetime upon doping the CdS samples with  $\text{Mn}^{2+}$  ions. The shortening of lifetime is less compared to the case of  $\text{Zn}_{1-x}\text{Mn}_x\text{S}$  (Sapra *et al*

2005). This is possibly due to a larger overlap of the emission spectra of the Mn  $d$  levels and the surface states in the case of  $\text{Cd}_{1-x}\text{Mn}_x\text{S}$ . Since the energy of the two emission channels is not so different, the extra stabilization gained by transferring an excitation to Mn  $d$  levels is not large here compared to the case of  $\text{Zn}_{1-x}\text{Mn}_x\text{S}$ , where the two energies were widely separated. However, some quenching of the surface state emission by Mn is still observed.

Figure 8 shows the fluorescence decay at 590 nm corresponding to the peak of the Mn  $d$  fluorescence emission. Apart from minor variations, the fast component of the fluorescence decay at 590 nm is the same in both the doped and undoped samples. Thus, this fast component is only due to the surface states in case of  $\text{Cd}_{1-x}\text{Mn}_x\text{S}$  nanocrystals similar to the earlier report (Sapra *et al* 2005) of  $\text{Zn}_{1-x}\text{Mn}_x\text{S}$  nanocrystals and Mn  $d$  levels have no contribution towards this fast component. It is interesting to note that at 590 nm, the shortening of lifetime upon doping is much less compared to that in figure 7. Obviously the extent of overlap between surface state emissions and Mn  $d$  levels is much larger at 590 nm than that at 510 nm; this further supports the previously made assumption that energy transfer between states reduces upon increase of overlapping of the involved states because of the lack of extra stabilization, normally achieved by the process. However, the lifetime data is not conclusive and to establish the slow decay from Mn  $d$  levels we have recorded a time delay spectrum. The intensity of the time delay spectrum is integrated between 100 nanoseconds and 1 microsecond after the excitation pulse. Thus, the fast processes that would have taken place within the first 100

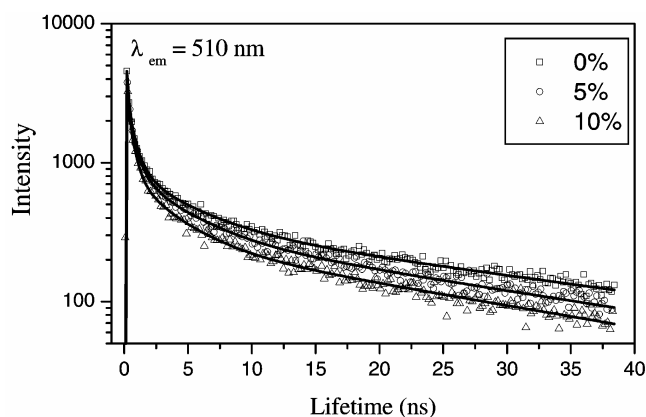


**Figure 7.** Fluorescence lifetime decay spectra recorded at 510 nm for undoped, 5% and 10% Mn-doped CdS nanocrystals synthesized at  $60^\circ\text{C}$ . The data were recorded at a resolution of 0.039 ns/channel. The PL decays were best fitted ( $\chi^2$  values  $< 1.2$ ) to four exponential functions. The five lifetimes (and amplitudes) are as follows: undoped CdS, 0.10 (0.65), 0.61 (0.24), 4.18 (0.07), 34.88 (0.04); 5% Mn-doped CdS, 0.09 (0.68), 0.59 (0.22), 3.76 (0.07), 30.08 (0.04); 10% Mn-doped CdS, 0.06 (0.72), 0.50 (0.21), 3.45 (0.05), 28.02 (0.03).

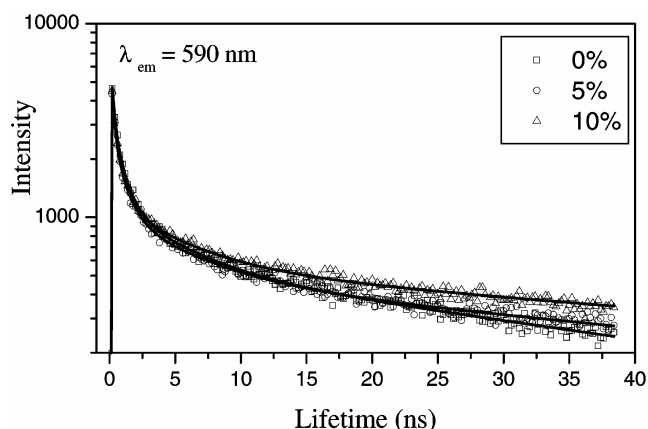


**Figure 8.** Fluorescence lifetime decay spectra recorded at 590 nm for undoped, 5% and 10% Mn-doped CdS nanocrystals synthesized at 60°C. The data were recorded at a resolution of 0.039 ns/channel. The PL decays were best fitted ( $\chi^2$  values < 1.2) to four exponential functions. The five lifetimes (and amplitudes) are as follows: undoped CdS, 0.14 (0.53), 0.78 (0.30), 4.67 (0.90), 45.30 (0.08); 5% Mn-doped CdS, 0.16 (0.58), 0.85 (0.26), 5.45 (0.09), 66.70 (0.07); 10% Mn-doped CdS, 0.11 (0.57), 0.72 (0.28), 5.19 (0.08), 81.64 (0.07).

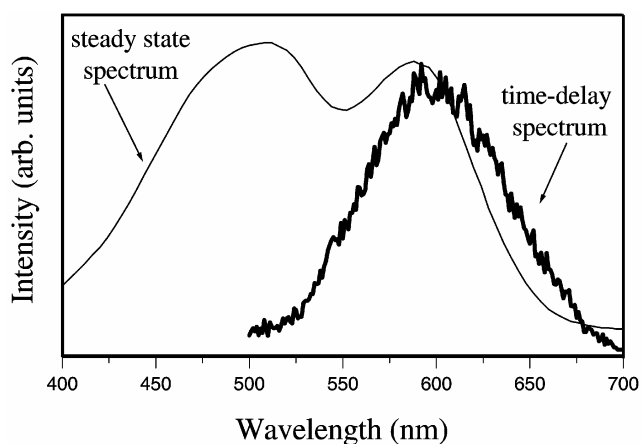


**Figure 9.** Steady state and time-delay fluorescence spectra for 5% Mn-doped CdS nanocrystals synthesized at 60°C.

nanoseconds are not observed in this spectrum. A comparison of the steady state spectrum with a spectrum recorded after a time delay is shown in figure 9 for the 5% Mn-doped CdS sample synthesized at 60°C. The time delay spectrum agrees quite well with the Mn  $d-d$  transition that causes emission at 590 nm with a complete absence of the 510 nm emission feature. Thus, the slow component of emission is attributed to Mn  $d-d$  transition. The fast component is the one that is seen in the steady state spectrum, but is absent in the time-delay spectrum. Thus, the fast component corresponds to the surface state emission centred at 510 nm. This clearly shows that Mn has a slow decay rate as in the bulk (Ehrlich *et al* 1985)

and that doping in nanocrystals does not shorten its decay time.

#### 4. Conclusions

We have synthesized different sized  $\text{Cd}_{1-x}\text{Mn}_x\text{S}$ , ranging from 18–33 Å by merely varying the synthesis temperature with varying Mn concentrations. Although, the starting Mn concentration is kept very high, a very small fraction of  $\text{Mn}^{2+}$  ions are incorporated into the CdS lattice. The EPR and XAS results show that  $\text{Mn}^{2+}$  ions are present in the nanocrystals, both inside the lattice and on the surface. With increasing temperatures, the  $\text{Mn}^{2+}$  ions shift towards the surface of the nanocrystals. The nanocrystals exhibit fast surface state and Mn  $d$  levels related long-lived fluorescence. Fluorescence decay profiles show that the lifetime of the surface state emission reduces upon doping, however, extent of shortening of the lifetime decreases with increased overlapping of the surface state emission with Mn  $d$  levels.

#### Acknowledgements

The authors thank the Department of Science and Technology for funding the project. One of the authors (DDS) acknowledges the National J. C. Bose Fellowship. (AN) acknowledges CSIR, Government of India, for a fellowship.

#### References

- Bhargava R N, Gallagher D, Hong X and Nurmikko A 1994 *Phys. Rev. Lett.* **72** 416
- Bocquet A E, Mizokawa T, Saitoh T, Namatame H and Fujimori A 1992 *Phys. Rev. B* **46** 3771
- Counio G, Gacoin T and Boilot J P 1998 *J. Phys. Chem. B* **102** 5257
- Ehrlich C, Busse W, Gumlich H E and Tschierse D 1985 *J. Crystal Growth* **72** 371
- Erwin S C, Zu L, Haftel M I, Efros A L, Kennedy T A and Norris D J 2005 *Nature* **436** 91
- Feltin N, Levy L, Ingert D and Pileni M P 1999 *J. Phys. Chem. B* **103** 4
- Furdyna J K 1988 *J. Appl. Phys.* **64** R29
- Guinier A 1963 *X-ray diffraction* (San Francisco, CA: Freeman)
- Hoffman D M *et al* 2000 *Solid State Commun.* **114** 547
- Levy L, Hocheppied J F and Pileni M P 1996 *J. Phys. Chem.* **100** 18322
- Mahadevan P and Sarma D D 2000 *Phys. Rev. B* **61** 7402
- Mikulec F V, Kuno M, Bennati M, Hall D A, Griffin R G and Bawendi M G 2000 *J. Am. Chem. Soc.* **122** 2532
- Nag A, Sapra S, Nagamani C, Sharma A, Pradhan N, Bhat S V and Sarma D D 2007 *Chem. Mater.* **19** 3252
- Ohno H 1998 *Science* **281** 951
- Ohno H 1999 *J. Magn. Magn. Mater.* **200** 110
- Pradhan N and Peng X 2007 *J. Am. Chem. Soc.* **129** 3339

- Sapra S and Sarma D D 2004 *Phys. Rev. B* **69** 165304
- Sapra S, Shanthi N and Sarma D D 2002 *Phys. Rev. B* **66** 205202
- Sapra S, Nanda J, Anand A, Bhat S V and Sarma D D 2003 *J. Nanosci. Nanotechnol.* **3** 392
- Sapra S, Prakash A, Ghanghrekar A, Periasamy N and Sarma D D 2005 *J. Phys. Chem. B* **109** 1663
- Soo Y L, Ming Z H, Huang S W, Kao Y H, Bhargava R N and Gallagher D 1994 *Phys. Rev. B* **50** 7602
- van der Laan G and Kirkman I W 1992 *J. Phys.: Condens. Matter* **4** 4189
- Viswanatha R, Sapra S, SenGupta S, Satpadi B, Satyam P V, Deb B N and Sarma D D 2004 *J. Phys. Chem. B* **108** 6303
- Vossmeier T, Katsikas L, Giersig M, Popovic I G, Diesner K, Chemseddine A, Eychmuller A and Weller H 1994 *J. Phys. Chem.* **98** 7665
- Wang Y, Herron N, Moller K and Bein T 1991 *Solid State Commun.* **77** 33